Available online at www.sciencedirect.com
SCIENCE DIRECT
Journal of Power Sources 146 (2005) 788–792
JOURNAL OF POWER SOURCES
www.elsevier.com/locate/jpowsour

Development of a high power lithium secondary battery for hybrid electric vehicles

J. Arai [a,*], T. Yamaki [a], S. Yamauchi [a], T. Yuasa [a], T. Maeshima [b], T. Sakai [b], M. Koseki [b], T. Horiba [b]

[a] *Hitachi Research Laboratory, Hitachi, Ltd., Ibaraki-ken 319-1292, Japan*
[b] *Hitachi Vehicle Energy, Ltd., Saitama-ken 369-0297, Japan*

Available online 27 April 2005

Abstract

A lithium secondary battery (Type II cell) for hybrid electric vehicles (HEV) was developed on the basis of previous battery techniques (Type I cell with amorphous carbon/$Li_{1+x}Mn_2O_4$). It used an improved cathode material and more advanced electrolyte. Cell performances of the Type II cell were evaluated and compared with a Type I cell of the same cell size, i.e. 40ϕ (diameter) $\times$108 mm (length). The Type II cell discharged 5.9 Ah, which was 1.5 times higher than the amount discharged by the Type I cell (3.8 Ah). The former had an input–output power of 800 W at 45% SOC (state of charge) and 25 °C, which was 1.3 times higher than that of the latter (600 W at around 40%). Moreover, the former had an input–output power of more than 100 W at −30 °C, though the Type I cell output power was only 50 W. A pulse charge–discharge cycle test with 167 W input and 260 W output for a 30–70% SOC range and a storage test at 50% SOC were carried out at various temperatures for the Type II cell. Less than a 15% DCR (direct current resistance) increase was observed in the pulse mode cycle test after 450 K cycles at 50 °C. No more than a 25% DCR increase was detected after 240 days in the 50% SOC storage test even at 65 °C. The activation energies for capacity change and DCR change in the storage test were also estimated for the Type II cell.
© 2005 Elsevier B.V. All rights reserved.

Keywords: HEV; Power density; Pulse cycle test; Storage test; Activation energy

1. Introduction

Large-scale lithium secondary batteries have been developed for energy-saving systems such as home-use load-leveling systems, stationary backup systems and electric vehicles (EV) including power-assist hybrid electric vehicles (HEV) [1–3]. EV and HEV applications are the most challenging ones to realize, because they require not only high energy density but also high power density [4]. We have developed a large-scale lithium secondary battery (Type I) employing a lithium manganese oxide cathode and an amorphous carbon anode for EV and HEV applications. The Type I cell (high power type) had an output density of more than 2000 W kg^{-1} and an energy density of 45 Wh kg^{-1} which are acceptable values for realization of HEV applications [3]. But, further progress in cell performance values is still required before large-scale lithium secondary batteries can be commercially marketed. Recently, we have developed the next step large-scale lithium secondary battery (Type II) for HEV applications by improving the cathode material and electrolyte.

This work presents the Type II cell performance values including charge–discharge capacities, input–output power properties, temperature dependency of input–output power, capacity and direct current resistance (DCR) behavior in the pulse mode charge–discharge cycle test and storage life test at various temperatures. We also evaluate the activation energies for capacity fading and DCR incrementing in the storage test.

* Corresponding author. Tel.: +81 294 52 7551; fax: +81 294 52 7632.
E-mail address: jarai@hrl.hitachi.co.jp (J. Arai).

0378-7753/$ – see front matter © 2005 Elsevier B.V. All rights reserved.
doi:10.1016/j.jpowsour.2005.03.087

2. Experimental

2.1. Cell preparation

Cylindrical shape test cells having a 40 mm diameter and 108 mm length were fabricated using a modified lithium manganese oxide cathode by substitutions of Mn with transition metals, an amorphous carbon anode, and $LiPF_6$ containing electrolyte for cell performance evaluation. The anode was prepared by coating and drying *N*-methyl pyrolidone (NMP) paste containing amorphous carbon and poly vinylidene fluoride (PVDF) on copper foil. The cathode was made in the same way, but on an aluminum foil and using a paste which contained modified lithium manganese oxide, PVDF and graphite carbon as electric conducting supporter [5]. Properties of principal materials used in the Types I and II cells, and cell size and weight are summarized in Table 1. The cathode material used in the Type II cell had about a 30% higher specific capacity than the cathode material used in the Type I cell. The electrolyte used in the former had a $3\,mS\,cm^{-1}$ higher conductivity than that in the latter.

2.2. Cell performance evaluation

Charge–discharge performances were measured using a Nittetsu Elex battery controller (5 V–200 A system). The charge–discharge capacities were recorded between 2.7 and 4.1 V with a 1 C rate current (3.6 A for Type I cell and 5.5 A for Type II cell). Direct cell resistances (DCR) were estimated using the *I–V* plots with 27, 55, and 100 A rate charge and discharge at various SOCs (states of charge). The limiting values of voltage in the charge and in the discharge were set as 4.16 and 2.5 V, respectively, for the estimation of maximum available currents. A pulse mode charge–discharge cycle test was done with the conditions of 167 W for input (charge) and 260 W for output (discharge) at 20, 40, and 50 °C. A storage test was carried out with a 50% SOC (3.65 V) at 0, 20, 40, 50, 65 and 80 °C. The DCR and discharge capacity were examined at appropriate intervals of the cycles or days.

Table 1
Specification of HEV test cells and material properties

Cell type	Type I	Type II
Specific discharge capacity of cathode material ($mAh\,g^{-1}$)	105	135
Conductivity of electrolyte ($mS\,cm^{-1}$, at 20 °C, 1 M $LiPF_6$)	9	11
Specific discharge capacity of anode material ($mAh\,g^{-1}$)	400	400
Cell size (mm)	$40\phi \times 108$	$40\phi \times 108$
Cell weight (mg)	300	310[a]

[a] Safety parts are adopted inside the cell.

3. Results and discussion

3.1. Type II cell performances

Fig. 1 shows the charge–discharge voltage curves as a function of cell capacity. The Type II cell had a similar discharge voltage curve to the Type I curve, though the capacity of the Type II cell was 1.5 times higher (5.9 Ah) than that of the Type I cell (3.8 Ah) due to the more favorable specific capacity density of the cathode material. The Type II cell needed shorter constant voltage (4.1 V) charging time than the Type I cell, indicating that the former had a better charging rate property.

Fig. 2 shows the input and output power properties evaluated for a 5-s charge and discharge as a function of SOC for both cells at 25 °C. The Type II cell had maximum output powers of 1400 W at 100% SOC and 1500 W at 0% SOC. Input power values in the Type II cell were much improved for low SOC (below 50%). The input and output curves of the Type II cell crossed at about 45% SOC. At this point, the Type II cell generated and regenerated more than 800 W,

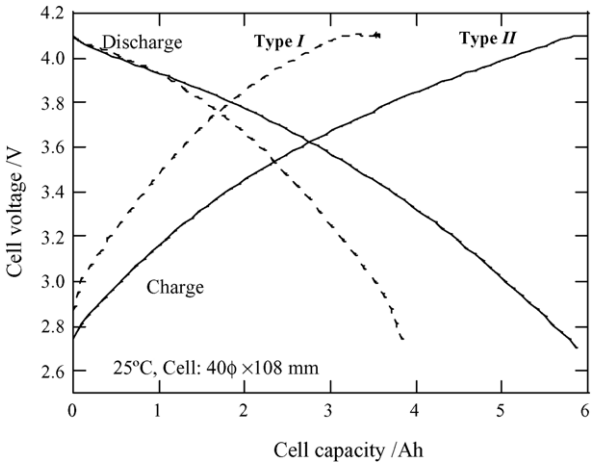

Fig. 1. Charge–discharge voltage curves of Types I and II cells at 25 °C.

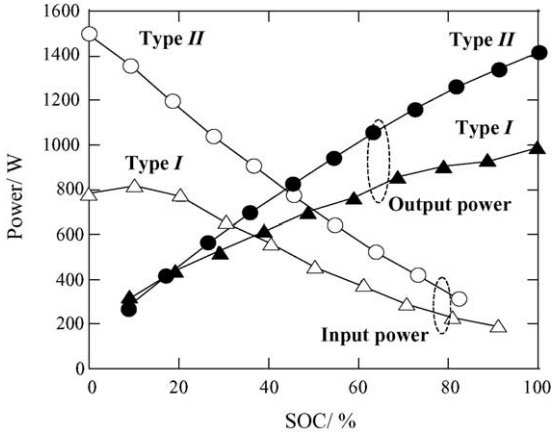

Fig. 2. Input and output power properties as a function of SOC for Types I and II cells at 25 °C.

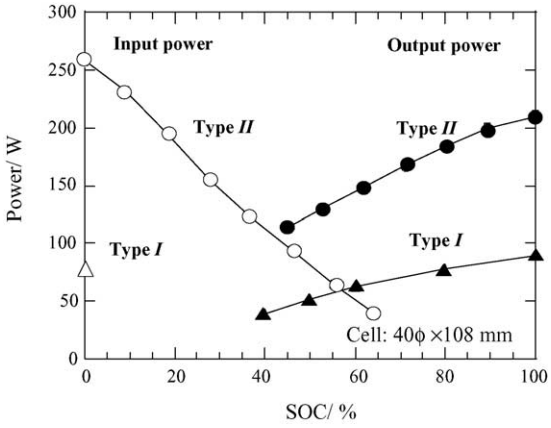

Fig. 3. Input and output power properties as a function of SOC for Types I and II cells at −30 °C.

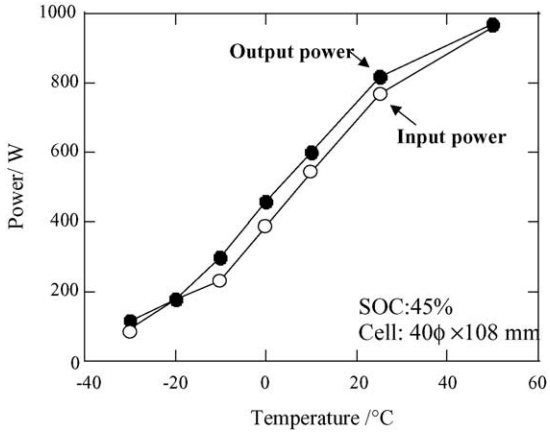

Fig. 5. Temperature dependency of the input and output power properties for Types I and II cells at 45% SOC.

which was 1.3 times higher than that of the Type I cell (600 W at 40% SOC). Supposing necessary input and output powers were 400 W cell^{-1} for an HEV system, we estimated the Type II cell could reserve 12 Wh cell^{-1} though Type I cell could only reserve 5.3 Wh cell^{-1}. Thus, the available energy of the Type II cell was more than two times higher.

Fig. 3 shows the input and output power properties evaluated for a 5-s charge and discharge as a function of SOC for the Types I and II cells at −30 °C. The Type II cell had an output power of more than 200 W at 100% SOC, which was two times higher than that of the Type I cell. The Type II cell had an output power of 250 W at 0% SOC and measurable values up to 65% SOC, though the Type I cell output power was only 75 W at 0% SOC. This was mainly due to the better electrolyte we used. Fig. 4 shows the ionic conductivities of the electrolytes for both cells as a function of temperature. The electrolyte for the Type II cell had higher conductivities than the electrolyte for Type I at all measured temperatures from −40 to 20 °C. The electrolyte used in Type II had a conductivity of 2.7 mS cm^{-1} at −30 °C, while the electrolyte for Type I had a value of 2 mS cm^{-1}. Fig. 5 shows temperature dependency of the input and output power properties for both cells at 45% SOC. Based on the plotted data of Figs. 4 and 5, we concluded temperature dependency of the power property was controlled by the ionic conductivity of the electrolyte in this cell system.

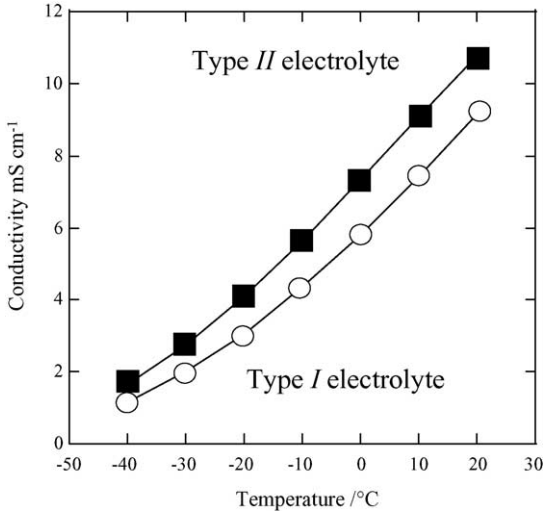

Fig. 4. Ionic conductivities of the electrolytes for Types I and II cells as a function of temperature.

3.2. Pulse mode charge–discharge cycle test

Fig. 6 shows the DCR change in the pulse mode charge–discharge cycle test for the Type II cell at various temperatures. The DCR increased no more than 15% at all test temperatures up to 450 K cycles (testing took more than 9 months), though a test temperature of 50 °C caused the DCR to increase at the beginning of the cycle test. The Type II cell showed a stable DCR during the test, meaning that the initial power would be sustained stably during the cycle test.

Fig. 7 shows the capacity change in the pulse mode charge–discharge cycle test for Type II cell at various

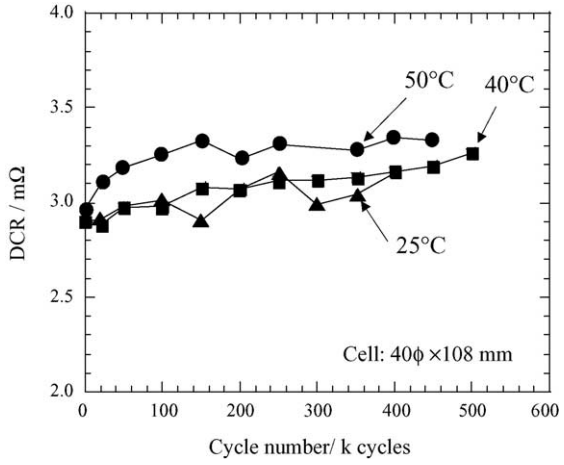

Fig. 6. DCR change in pulse mode charge–discharge cycle test for Type II cell at various temperatures.

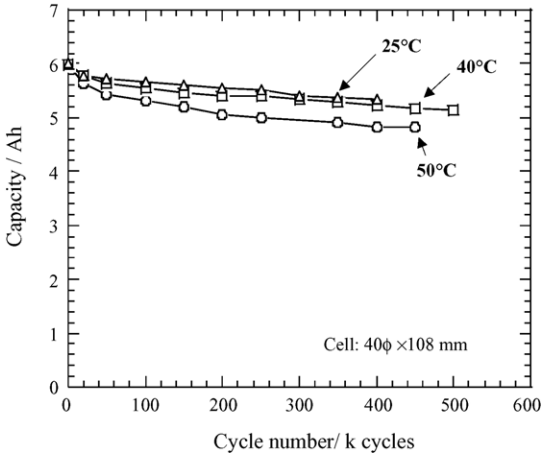

Fig. 7. Capacity change in the pulse mode charge–discharge cycle test for Type II cell at various temperatures.

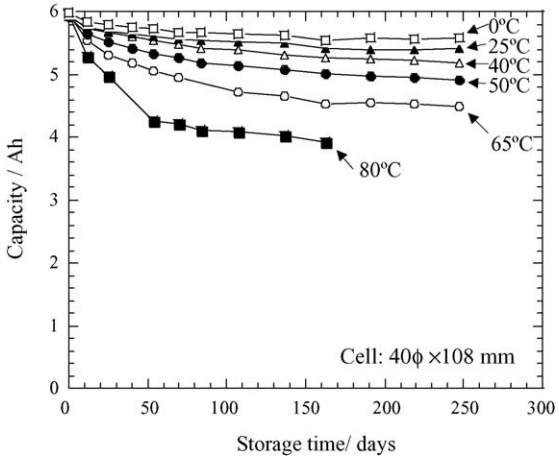

Fig. 9. Capacity change in the storage test for Type II cell at various temperatures and 50% SOC.

temperatures. The Type II cell kept its capacity within 80% at 50 °C, 87% at 40 °C, and 90% at 25 °C of the initial values up to 450 K cycles. Thus, we found the Type II cell showed good stability regarding its power and available energy during the cycle test.

3.3. Storage life test

Fig. 8 shows the DCR change in the storage test for Type II cell at various temperatures and 50% SOC. No increase was observed in DCR when the cell was stored at 0 and 25 °C after 240 days. Only 5, 13, and 21% DCR increases were detected after 240 days, when the cell was stored at 40, 50 and 65 °C, respectively. Furthermore, the Type II cell kept the increase in DCR below 40% when it was stored at 80 °C.

Fig. 9 shows the capacity change in the storage test for Type II cell at various temperatures and 50% SOC. The Type II cell sustained capacities within 93, 91, 87, 82 and 75% after being stored 240 days at 0, 25, 40, 50 and 65 °C, respectively. Furthermore, when the cell was kept at 80 °C for more than 160 days, 65% of the initial capacity was retained. The Type II cell expanded the possibility of HEV applications for the lithium secondary battery by improving the temperature tolerances.

Liaw et al. [6], analyzed the capacity change in the cycles tests by the Arrhenius equation and estimated the activation energy for capacity fading. Fig. 10 shows the Arrhenius plot of logarithmic capacity fading (ΔQ) versus reciprocal temperature for the Type II cell at 50% SOC. The curves had good linearity and gave activation energies of 26.5, 31.9, 27.7 and 25.6 kJ mol^{-1} at evaluated intervals of 12, 54, 107 and 163 days, respectively. Liaw et al. reported that the activation energies for capacity were 50–55 kJ mol^{-1} and they were related to heat generation in the charge–discharge process. The activation energies we estimated were smaller than those of Liaw et al. A possible reason for this difference might be the cell size (their cells were 18$\phi \times 65$ mm), considering that capacity fading was affected by the cell heat generation. The large cylindrical cell had a relatively smaller surface area

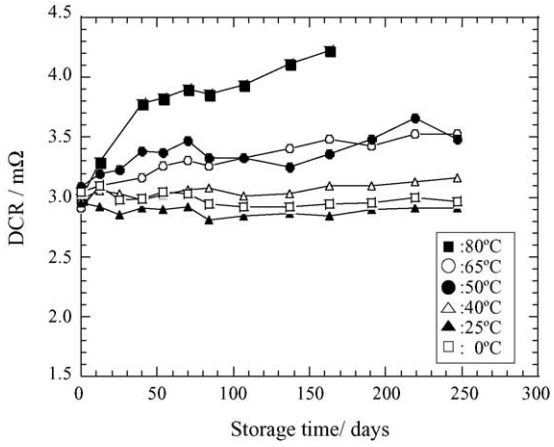

Fig. 8. DCR change in the storage test for Type II cell at various temperatures and 50% SOC.

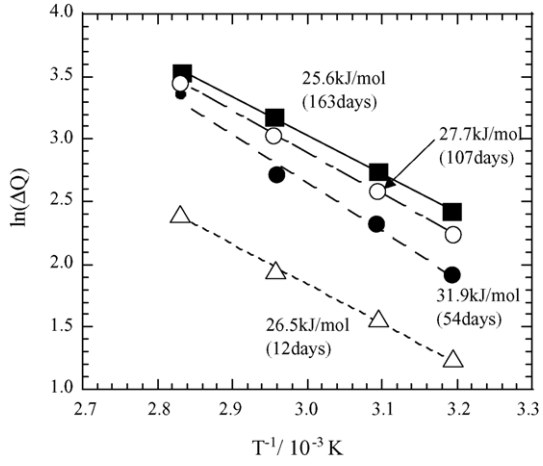

Fig. 10. Arrhenius plot of logarithmic capacity fading vs. reciprocal temperature for Type II cell at 50% SOC.

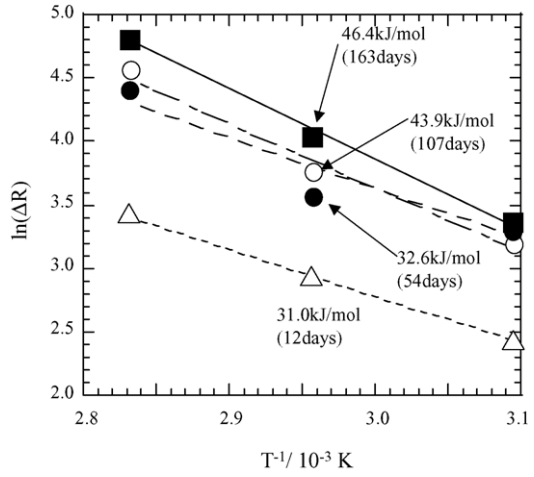

Fig. 11. Arrhenius plot of logarithmic DCR increase vs. reciprocal temperature for Type II cell at 50% SOC.

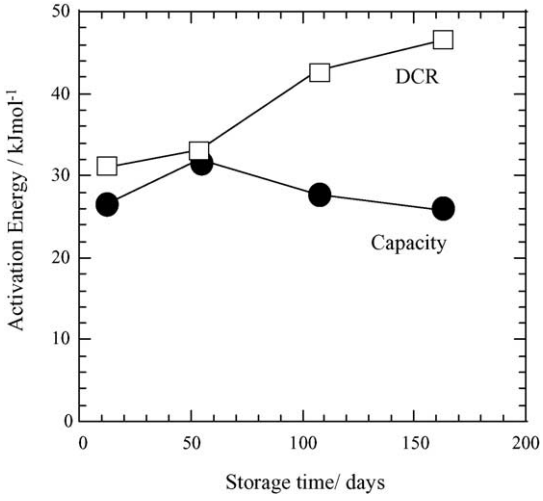

Fig. 12. Change in activation energy for DCR and capacity fading during the storage test for Type II cell.

than the small cell, depressing the heat diffusion efficiency and leading to capacity fading. This fact indicated that heat management of the cell was important for good cell life.

Fig. 11 shows the Arrhenius plot of the logarithmic DCR increase (ΔR) versus reciprocal temperature for the Type II cell at 50% SOC. The curves had good linearity, giving activation energies of 31.0, 32.6, 43.9 and 46.4 kJ mol^{-1} at evaluation intervals of 12, 54, 107 and 163 days, respectively. The activation energies for DCR increase increased with storage time, indicating that DCR increase rate decreased with storage time. These values were similar to the activation energy reported by Liaw et al.: 32.2 kJ mol^{-1} after 12 weeks. These results suggested that DCR charge was not affected by cell size or heat diffusivity.

Fig. 12 shows the change in activation energies for DCR increase and capacity fading during the storage test for the Type II cell. The activation energies for capacity fading stayed almost constant for 163 days. But, the activation energies for DCR increase rose after 54 days. This meant that the DCR increase rate slowed down after about 50 days, though the initial degradation rates for the capacity and DCR were almost the same. These results also suggested the causes of degradation of the capacity and DCR were not the same. The analysis of cell life test results using the Arrhenius plot provided useful information concerning reactions inside the cell just as the direct observation of the electrodes by using spectroscopic methods can provide. We are going to study the degradation mechanism by this method and try to predict cell life.

4. Conclusions

We have developed a next step large-scale lithium secondary battery (Type II) for HEV application and evaluated its cell performances. We found the Type II cell performances were much improved compared to the earlier Type I cell. The former discharged 5.9 Ah cell^{-1}, which was 1.5 times higher than that of the latter and the former had an input–output power of 800 W cell^{-1}, which was 1.3 times higher. At –30 °C, the Type II cell had an input–output power of 100 W cell^{-1} which was two times higher. Moreover, the pulse cycle life test showed only a small increase of DCR in 450 K cycles. Good durability at 80 °C was also demonstrated. We think the Type II cell is a promising battery for HEV applications.

References

[1] K. Takei, K. Ishihara, K. Kumai, T. Iwahori, K. Miyake, T. Nakatsu, N. Terada, N. Arai, J. Power Sources 119–121 (2003) 887.
[2] K. Adachi, H. Tajima, T. Hashimoto, K. Kobayashi, J. Power Sources 119–121 (2003) 897.
[3] K. Tamura, T. Horiba, T. Iwahori, J. Power Sources 81–82 (1999) 156.
[4] R. Spotnitz, in: W.A. Schalkwijk, B. Scrosati (Eds.), Advances in Lithium-Ion Batteries, Kluwer Academic/Plenum Publishers, New York, 2003, p. 433.
[5] J. Arai, J. Electrochem. Soc. 150 (2003) A219.
[6] B.Y. Liaw, E.P. Roth, R.G. Jungst, G. Nagasubramanian, H.L. Case, D.H. Doughty, J. Power Sources 119–121 (2003) 874.